Exploring the Magnéli Phase of Transition Metal Oxides: A Promising Frontier for Thermoelectric Advancements

Mostafa M. Elkady
Department of Interdisciplinary Engineering Sciences, Interdisciplinary Graduate School of Engineering Sciences, Kyushu University

Ohtaki, Michitaka
Department of Interdisciplinary Engineering Sciences, Interdisciplinary Graduate School of Engineering Sciences, Kyushu University

https://doi.org/10.5109/7157998

出版情報：Proceedings of International Exchange and Innovation Conference on Engineering & Sciences (IEICES). 9, pp.334-342, 2023-10-19. 九州大学大学院総合理工学府
バージョン：

Exploring the Magnéli Phase of Transition Metal Oxides: A Promising Frontier for Thermoelectric Advancements

Mostafa M. Elkady [1*], Michitaka Ohtaki[1,2]

[1] Department of Interdisciplinary Engineering Sciences, Interdisciplinary Graduate School of Engineering Sciences, Kyushu University, Kasuga, Fukuoka, 816-8580, Japan

[2] Transdisciplinary Research and Education Center for Green Technologies, Kyushu University, Kasuga, Fukuoka 816–8580, Japan

*Corresponding author email: mostafa.kadi22@gmail.com

Abstract: *Thermoelectric materials convert heat energy into electrical energy. They have the potential to be used in a variety of applications, including power generation, waste heat recovery, and temperature control. Several transition metal suboxides, also known as Magnéli phases, are a promising class of thermoelectric materials because of their high electrical conductivity, low thermal conductivity, and chemical stability. In this review article, we discuss the Magnéli phase of five different transition metal suboxides: titanium suboxide (TiO_x), tungsten suboxide (WO_x), molybdenum suboxide (MoO_x), vanadium suboxide (VO_x), and niobium suboxide (NbO_x). We focus on their crystal structure, electrical and thermal properties, and potential applications as thermoelectric materials. We conclude that the Magnéli phases have the potential to be high-performance thermoelectric materials. However, further research is needed to optimize their properties and develop new synthesis methods.*

Keywords: *thermoelectric, Magnéli phase, transition metal suboxides*

1. Introduction:

Renewable energy resources and energy-efficient technologies are important for the future energy revolution. Thermoelectric technology allows for direct conversion of heat energy into electrical energy. The thermoelectric effect is used in thermoelectric modules, which are assembled into thermoelectric generators. Although thermoelectric generators have proven to be reliable in the past, affordable and non-toxic materials are required to expand their role in the future [1]. In 1821, the Seebeck effect was discovered, which creates an electromotive force in a circuit when there is a temperature difference at the joint of two metals. The generated current and electromotive force are related to this phenomenon. The voltage difference (ΔV) increases with the temperature difference (ΔT) between metal joints. The Seebeck coefficient is a property-based constant that varies among materials, with metals having a low coefficient of about several μV/K and semiconductors having a high coefficient of about 200 μV/K [2].

The Seebeck coefficient (a) is defined as

$$\alpha = \frac{\Delta V}{\Delta T} \qquad (1)$$

where ΔV represents voltage difference in volts, while ΔT represents temperature difference in Kelvin. The performance of a material is described by the dimensionless quantity called the figure of merit (ZT), which reflects the requirements for a good thermoelectric material. The challenge in thermoelectric research since the late 50s has been to increase ZT of materials which includes both electrical and thermal properties, as shown in equation (2).

$$zT = \frac{\alpha^2 \sigma}{k} T \qquad (2)$$

A perfect thermoelectric material has glass-like thermal conductivity and crystal-like electronic transport capabilities, satisfying the idea of a "phonon-glass electron-crystal" described by Slack [3].

Another property is called thermal conductivity (k) which is caused by lattice vibrations (phonons) and heat-carrying charge carriers. It can be described as

$$k = k_{lat} + k_{el} \qquad (3)$$

which k_{lat} is the lattice thermal conductivity and k_{el} is the electronic thermal conductivity.

The k_{el} can be calculated with the Wiedemann-Franz law stating that the ratio of the electronic part of thermal conductivity (k_{el}) to electrical conductivity (σ) in a metal is proportional to temperature (T) [4].

$$k_{el} = L\sigma T \qquad (4)$$

Theoretically, the proportionality constant L, known as the Lorenz number, is equal to

$$L = \frac{k}{\sigma T} = \frac{\pi^2}{3}\left(\frac{k_B}{e}\right)^2 = 2.44 \times 10^{-8}\ V^2K^{-2} \qquad (5)$$

where k_B is Boltzmann's constant, and e is the elementary charge. The Wiedemann-Franz law shows that the ratio of thermal conductivity to electrical conductivity, κ/σ, is constant for different metals under the same temperature [5].

Thermoelectric oxides are gaining attention for their stability, cost-effectiveness, and eco-friendliness. They offer the potential for high-temperature applications and can convert thermal gradients into electricity [6]. Layered cobaltite like Na_xCoO_2 and $Ca_3Co_4O_9$ [7] as well as other families of thermoelectric oxides including zinc oxide (ZnO), perovskites, and tungsten bronze structured oxides are showing high-temperature stability. ZnO has the highest n-type ZT values and sodium cobaltite has the highest p-type ZT values among all oxide candidates [8]. Other oxide materials like α and γAl_2O_3 doped sintered ZnO and sintered $CuAlO_2$ also have high thermoelectric properties [9, 10]. Although oxide materials have lower thermoelectric properties compared to compounds containing elements like tellurium and antimony, they are suitable for high-temperature applications because of their superior stability in oxidizing environments [10].

Among metal oxides, Magnéli phase oxides, including titanium and tungsten, have the potential for thermoelectric use because of their low thermal conductivities and metallic-like electrical conductivities [11]. Arne Magnéli is a pioneer in researching transition metal sub-oxides and shear plane dislocations. His research led to the discovery of conductive Titanates and perovskites. He studied Tungsten, Molybdenum and Titanium sub-oxides and found dislocation planes in their crystalline structure, which accounted for their electrical conductivity and lubricious properties. This mechanism is also observed in graphite and graphene. Magnéli phases have semi-metallic characteristics and similar electrical properties to carbon. Because of the demand for inert conductive materials, there is significant research being done on Magnéli materials [12]. Magnéli et al. investigated transition metal oxides using XRD. They found comparable compositions expressed by Ti_nO_{2n-1} (n=2, 3,...etc.) and expected that they may be formed from the rutile structure. They proposed the crystallographic shear structure principle, which involves dividing the main structure into blocks parallel to a shear plane (Fig. 1a), translating the blocks relatively by shear vector (Fig. 1b), and removing overlapping parts as shown in (Fig. 1c) [13-15].

The partial reduction of certain transition metal oxides leads to crystallographic shear planes with altered metal linkage and retained octahedral coordination. Shear planes are observed in oxides based on ReO_3 and rutile structures with changes in corner/edge sharing to edge/face sharing. The structural changes in rutile with increasing oxygen deficiency reveal regular arrays of shear planes forming "shear compounds". Shear planes are present even with low oxygen deficiencies [16]. In this review article, an elaborate and comprehensive discussion will be presented on the Magnéli phase of five different transition metal suboxides, TiO_x, WO_x, MoO_x, VO_x, and NbO_x with a special focus on their potential application as thermoelectric materials.

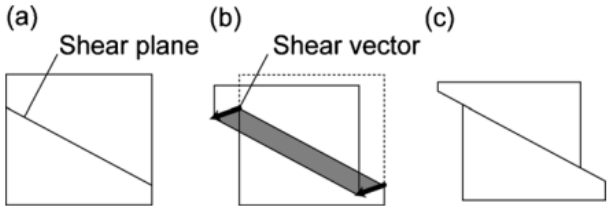

Fig. 1: schematic diagram of crystallographic shear operation. Reprinted from [13], with the permission of AIP Publishing.

2. Titanium suboxides Magnéli phases

Magnéli phases for TiO_x are a class of sub-stoichiometric titanium oxides with a chemical formula of Ti_nO_{2n-1}, where *n* varies from 3 to 9 (and more typically between 4 and 6) [17, 18]. Despite all three forms of Titanium oxides (rutile, anatase, and brookite) being composed of TiO_6 octahedron basic units, their frameworks differ, resulting in distinct properties for each crystal [19]. Arne Magnéli first investigated the Magnéli phase of TiOx in the 1950s, after developing a phase diagram of a Ti-O system [20]. The Magnéli phase is formed by the crystalline lattice of rutile TiO_2, in which a lack of oxygen results in delocalized electrons in the d band [21]. The recent focus on these materials is a result of their exceptional electrical conductivity, chemical stability, and remarkable ability to resist corrosion [21]. TiO_x shows a triclinic crystal structure and is considered to be a mixed-valence compounds due to the presence of both Ti^{4+} and Ti^{3+} ions in their compositions [21]. Also, TiO_x exhibits a remarkable level of conductivity, particularly for values of *n* equal to 3, 4, and 5, after which there is a decline in conductivity for larger *n* values [18].

Magnéli phases are difficult to obtain in a pure form due to their similar lattice parameters [12]. The Magnéli phase crystal lattice can be understood by comparing it with the crystal lattice of TiO_2. The formation of TiO_2 phases is explained by changes in the octahedral packing of TiO_2 due to the removal of O atoms. Oxygen defects distort [TiO_6] octahedral structure, leading to Magnéli phase formation with increasing defect concentration. Magnéli-phase crystal structure has TiO_2 octahedra blocks with an oxygen deficiency for each n^{th} layer, resulting in shear planes in the structure where the 2D chains become face-sharing. This reduces the symmetry of the crystal system from tetragonal to triclinic as the unit cell size increases [22, 23]. The crystal structures of TiO_x including Ti_3O_5 [24, 25], Ti_4O_7[26, 27], Ti_5O_9 [28, 29], Ti_6O_{11} [28, 30, 31], Ti_7O_{13}, Ti_8O_{15}, and Ti_9O_{17} [28, 30] are shown in Fig. 2.

γ-Ti_3O_5 displays metallic behavior, whereas δ-Ti_3O_5 exhibits semiconducting properties. The transition

between the two phases is induced by a Mott-Hubbard metal-insulator transition, and the alteration in electrical conductivity is due to a disconnection in the conducting pathways within the crystal [24]. Both Ti_4O_7 and Ti_5O_9 are oxides with mixed valence states. Ti_4O_7 has equal numbers of Ti^{4+} and Ti^{3+} positions, while Ti_5O_9 has a 3:2 ratio of Ti^{4+} to Ti^{3+} positions. These oxides have structures similar to rutile and contain rutile-like blocks that are infinite in x and y dimensions [32].

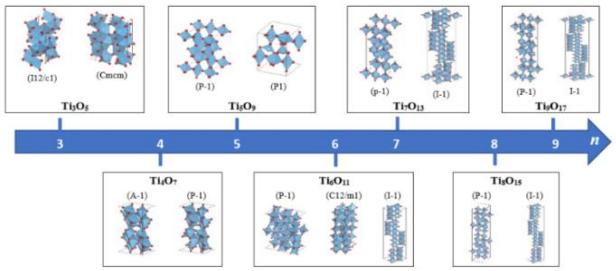

Fig. 2: Crystal structure of Titanium suboxides.

Harada et al. [13] synthesized and examined the thermoelectric properties of Ti_nO_{2n-1} which was synthesized by solid-state reaction followed by hot pressing in a carbon die. All sub-stoichiometric specimens are Magnéli phases, with regularly introduced crystallographic shear planes. Electrical conduction is *n*-type, with higher carrier concentration and lower electrical resistivity and Seebeck coefficient for greater oxygen deficiency. Lattice thermal conductivity decreases with oxygen deficiency, which indicates that crystallographic shear planes scatter phonons but not carriers. The hot-pressed $TiO_{1.90}$ had the highest thermoelectric ZT of 0.13 at 773 K [13]. Temperature dependence of electrical conductivity, Seebeck coefficient and ZT of some TiO_x (x=1.95, 1.9, 1.85, and 1.8) were shown in Fig. 3. In addition, H. Lee et al. [33] deposited TiO_x with sub-stoichiometric composition via the atmospheric plasma spray method, using varying H_2 gas ratios in the torch hardware. Oxygen deficiencies increase electrical conductivity but decrease Seebeck coefficient. The material has reduced thermal conductivity due to the presence of pores and interfaces. $TiO_{1.93}$ material had a ZT value of 0.132 at 750 K. L. Hao et al. [34] used Spark plasma sintering (SPS) followed by carbon reduction to create Magnéli phase Ti_nO_{2n-1} composites. the value *n* depending on the reduction temperature and holding time. With increasing holding time, the amount of TiO increased while the amount of Ti_3O_5 decreased. Ti_9O_{17} and Ti_8O_{15} were formed at 10 h holding time, and Ti_3O_5 phase was also formed at 15 and 20 h holding time. Compared to rutile TiO_2 prepared by SPS, the thermoelectric properties were considerably enhanced, including electrical conductivity, thermal conductivity, Seebeck coefficient, power factor (PF), and ZT value. At 20 hours of holding time, the samples achieved a maximum PF of 6.5×10^{-4} $Wm^{-1}K^{-2}$ at 973 K and a maximum ZT value of 0.1 at 873 K [34]. Another Magnéli phase of Ti_5O_9 ceramics were made by hot press solid-state reaction between anatase TiO_2 nanopowder and Ti powder at 950 ℃ and 40 MPa. A small polaron hopping mechanism causes electrical conductivity to change with temperature. Vibrational entropy during polaron hopping is negligible, and data can be explained with a modified Heikes–Chaikin–Beni formula. ZT value was 0.3 at 1076 K [35].

Yuan, Z., et al. [19] synthesized Reduced $Ti_{1-x}Nb_xO_{2-\delta}$ ceramics using a solid-state process, followed by 10 hour annealing in a reducing H_2 environment at 1573 K. They showed that the resistivities decreased with temperature and showed semiconductor behavior, while increasing Nb doping levels increased resistivities for fixed temperatures. Seebeck coefficients were negative, indicating electron carriers, and increased gradually with higher Nb doping levels. Small polaron conduction was observed in electrical transport, however, thermal conductivities increased with temperature, with lattice thermal conductivity being the predominant contributor. At 380 K, the Nb doping level with x = 0.20 produced the greatest ZT value of 0.016, about 2.9 times greater than the undoped TiO2 sample. Similarly, $Ti_{1-x}Nb_xO_{2-\delta}$ was synthesized using a standard solid-state reaction approach, but it was then annealed for 10 hours at 1473 K in a reducing environment of 90%Ar-10%H_2. At 380 K, the greatest ZT value of 0.023 was found for x=0.01, which is 2.6 times more than the undoped TiO_2 sample [36]. D. Zhou et al. [37] used a high-pressure and high-temperature (HPHT) approach to incorporate Ta into TiO_2. Ta reduced TiO_2 to Magnéli phase TiO_x (mostly Ti_8O_{15}) and produced sub-micron Ta_2O_5. The addition of Ta inhibited grain growth. The sample's hardness and conductivity increased while the Seebeck coefficient, lattice thermal conductivity, and total thermal conductivity decreased. This synergistic optimization was achieved with increased Ta addition. At 973 K, the maximum ZT value of the composite ceramic was 0.176. Moreover, They added Nb to TiO_2 using HPHT. The optimal Nb concentration was found to be x=0.23. The composite ceramics consisted of TiO_2, Ti_4O_7, NbO_2, and NbO, with a unique nanometer pore structure appearing on the grain of the sample. The thermoelectric properties of the samples were influenced by NbO, with a significant increase in thermal conductivity and 'metallic conductive behavior at high concentrations. Repeated high-temperature testing reduced the NbO phase, leading to a composite NbO_2 and Ti_4O_7 phase with improved ZT value and reduced thermal conductivity. The maximum ZT value obtained was 0.313 at 973 K after repeated high-temperature tests [38]. M. Mikami et al. [39] investigated the thermoelectric characteristics of TiO_2 with oxygen defects as well as the $Ti_n(O, N)_{2n-1}$ Magnéli phase. The mixing ratio of TiO_2 and

TiN can be changed to adjust oxygen deficiency and the n index of the Magnéli phase. Oxygen shortage promotes electron doping, which dramatically lowers. Seebeck coefficient decreases with electron doping, yet the PF value increases at high temperatures due to the absolute value of Seebeck coefficient and the temperature increase. The nanometer-order periodic planar defect structure of the Magnéli phase can aid phonon scattering and lowering. The Ti_7O_{13} Magnéli phase sample had an estimated ZT value of 0.4 at 1150 K.

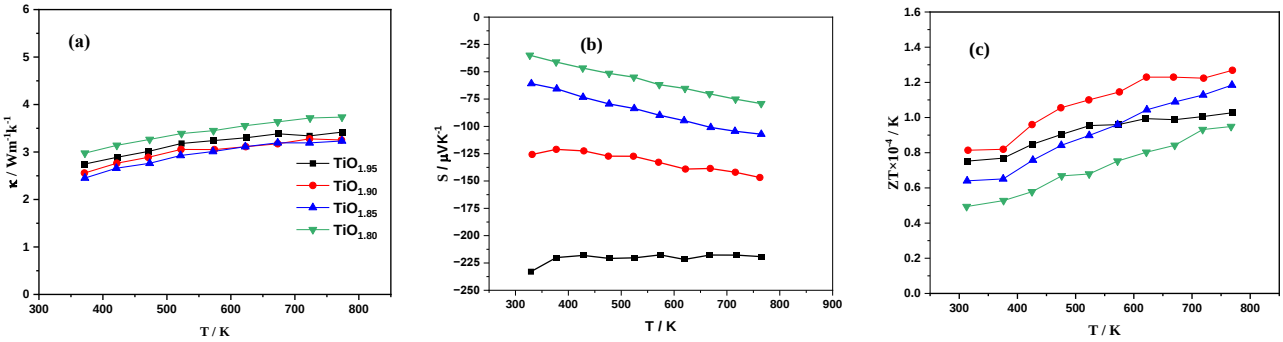

Fig. 3: Temperature dependence of (a) electrical conductivity (b) Seebeck coefficient (c) ZT of TiO_x. Reprinted from [13], with the permission of AIP Publishing.

3. Tungsten suboxides Magnéli phases

There are several sub-stoichiometric structures of WO*x*, (2 < x < 3) and the crystal structures of Magnéli phases are monoclinic for $W_{18}O_{49}$, $W_{20}O_{58}$, $W_{17}O_{47}$, and $W_{25}O_{73}$, orthorhombic for $W_{32}O_{84}$ and W_3O_8, and tetragonal for W_5O_{14} [40] as shown in Fig. 4. An intriguing method involves using crystallographic shear (CS) to decrease lattice thermal conductivity k_{lat} by boosting phonon scattering. CS plane structures emerge when a transition metal is partially reduced, and oxygen layers are removed from the structure. In the tungsten-oxygen system, insulating ReO_3-type WO_3, semiconducting phase $W_{20}O_{58}$ with CS planes, metallic phase $W_{18}O_{49}$ with pentagonal columns (PC), and metallic rutile-type WO_2 are seen with varying coupling of the [WO_6] octahedral [41].

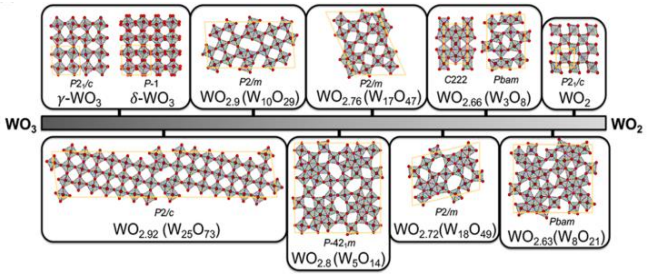

Fig. 4: Crystal structures of tungsten oxides. Reprinted (adapted) with permission from [42]. Copyright 2023 American Chemical Society.

Kaiser et al. [41] investigates the solid-state reaction of tungsten oxides with tungsten in the composition range of WOx (2.50 ≤ x ≤ 3) during spark plasma sintering (SPS).

$$\frac{x}{3}WO_3 + \left(1 - \frac{x}{3}\right)W \rightarrow WO_x \qquad (6)$$

They revealed the formation of a new phase "$WO_{2.82}$" between 2.72 ≤ x ≤ 2.90, which might have the composition $W_{12}O_{34}$. The thermoelectric properties of the materials are continuously tunable with the oxygen-to-tungsten ratio. The lattice thermal conductivity is significantly reduced until 700 K for the sample with the composition x = 2.84, which contains the phases $W_{18}O_{49}$ and "$WO_{2.82}$". the introduction of multiple phases is a way for reducing the thermal conductivity due to increased phonon scattering at the phase interfaces. For high-temperature applications, CS planes might be fewer phonon scattering centers. ZT of WO_x were shown in Fig. 5a.

Tran et al. [43] synthesized Single phase $W_{18}O_{49}$ directly from WO_3 and WO_2 via reactive SPS, which is faster than conventional methods. The reaction between WO_3 and WO_2 is more suitable than WO_3 and metal W powder because of similarities in the coordination environment. Anisotropic thermoelectric properties and the effect of applied pressure (perpendicular or parallel) were observed in the synthesized samples, resulting in low thermal conductivity. ZT was increased to 0.08 at 1073 K for the sample sintered under 50 MPa pressure as shown in Fig. 5b. So, $W_{18}O_{49}$ shows metallic behavior and promises to be a cost-effective n-type thermoelectric material. They also investigated the high-temperature thermoelectric characteristics of $(W_{1-x}Ti_x)_{18}O_{49}$ [44]. The undoped $W_{18}O_{49}$ sample exhibited metallic behavior with high electrical conductivity and a low Seebeck coefficient. Ti substitution at the W site decreased carrier concentration while increasing Seebeck coefficient and thus PF at high temperatures up to x = 0.2. The top ZT value was 0.50 at 1073 K for x = 2, while the lowest ZT value was 0.20 0.03 at 1073 K (x = 0.1). Ti dopant has a solubility limit between x=0.1 and x=0.15, limiting performance increase via carrier concentration tweaking for the inherently overdoped $W_{18}O_{49}$-based oxide. In addition, Kieslich et al. used SPS to synthesize $W_{1-x}Ta_xO_{2.90}$. The reduction in thermal conductivity of Ta-containing samples was achieved by adding Ta_2O_5 to the WO_3/W reaction mixture. The addition

resulted in a 30% decrease in thermal conductivity over the measured temperature range. This was due to phonon scattering by shear planes and micron-sized inclusions. The electronic properties were not affected by the substitution, which ultimately led to an enhancement in thermoelectric performance and a relatively high ZT value of 0.15 at 1100 K for n-type metal oxides [45].

4. Molybdenum suboxides Magnéli phases

Like WO_x, there are several sub-stoichiometric structures of MoO_x, ($2 < x < 3$) as shown in Fig. 6. Mo_9O_{26} and Mo_8O_{23} [46] have edge-sharing [MoO_6] octahedrons, while Mo_5O_{14} [47] and $Mo_{17}O_{47}$ [48] have pentagonal MoO_7 bipyramids with edge-shared MoO_6 octahedrons. Mo_4O_{11} has a unique structural motif of corner-sharing MoO_6 octahedrons and MoO_4 tetrahedrons and it demonstrated exceptional efficacy as a composite electrocatalyst for the methanol oxidation reaction (MOR) [49].

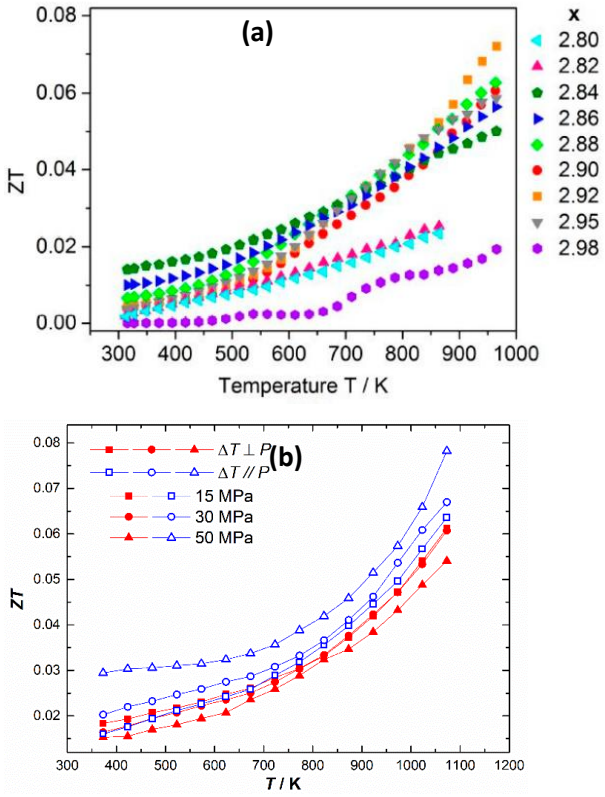

Fig. 5: Temperature dependence of ZT (a) WO_x samples ($2.80 \leq x \leq 2.98$) [41] (b) P // and ⊥ directions for $W_{18}O_{49}$ [43]

The stoichiometric phases of molybdenum oxide have different crystal structures, with α-MoO_3 having a van der Waals layered orthorhombic structure and β-MoO_3 having a monoclinic structure [42, 50]. The Magnéli phase Mo_8O_{23}, on the other hand, displays a superlattice modulation that is likely caused by a concerted pairwise rotation of [MoO_6] octahedra in the perovskite Mo_4O_{15} layers [3]. Conversely, Mo_4O_{11} exhibits a resistivity abnormality that is attributed to a charge density wave associated with partial nesting of Fermi surfaces. These investigations exemplify the diverse properties and behaviors of Molybdenum Magnéli phases.

Khailla et al. [51] measured the electrical conductivity and Seebeck coefficient of MoO_3, MoO_2, Mo_4O_{11}, Mo_8O_{23}, Mo_9O_{26}, $Mo_{13}O_{38}$, and $Mo_{17}O_{47}$ up to 300 °C. It has been observed that the conductivity value increases at room temperature when there is deviation from stoichiometry. So, MoO_3 and its suboxides display semiconductor behavior. At low temperatures, MoO_2 exhibits a semimetal-like character of $10^{-2}\,\Omega^{-1}cm^{-1}$ instead of a semiconductor. The thermoelectric power shows that oxides are n-type semiconductors up to 300°C. Kaiser et al. [52] prepared MO_x ($2 \leq x < 3$) from α-MoO_3 and Mo powder via SPS. The synthesis of $Mo_{18}O_{52}$, $Mo_{17}O_{47}$, and γ-Mo_4O_{11}, despite their narrow composition ranges, resulted in single-phase products. Among these products, $Mo_{17}O_{47}$ exhibited the highest PF. On the other hand, $Mo_{18}O_{52}$ proved to be an intrinsic narrow-gap semiconductor with extremely low thermal conductivity across the entire temperature range. It also displayed a high p-type Seebeck coefficient at room temperature and a p−n transition at 440 K. In contrast, MoO_2, γ-Mo_4O_{11}, and $Mo_{17}O_{47}$ demonstrated poor metallic conductivity. Additionally, a new reversible transition was discovered at 450 K through specific heat measurements in γ-Mo_4O_{11}.

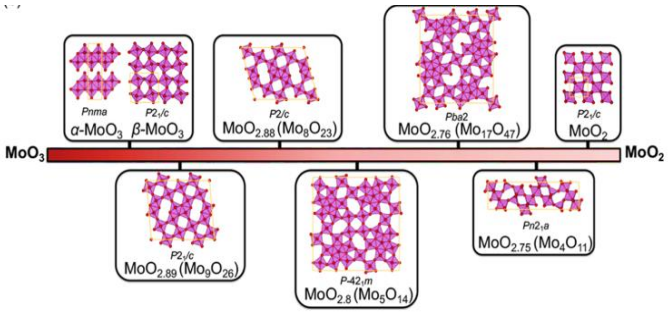

Fig. 6: Crystal structure of molybdenum oxides and molybdenum suboxides. Reprinted (adapted) with permission from [42]. Copyright 2023 American Chemical Society.

5. Vanadium suboxides Magnéli phases

In the crust of the Earth, vanadium ranks sixth among transition metals and is the 20th most common element. Some literature suggests it's the fourth most abundant after iron, titanium, and manganese [53]. The mixed-valence vanadium oxides can be categorized into two series: Magnéli and Wadsley. V_3O_7 and V_6O_{13} in the Wadsley series undergo a phase transition at 5.2 K and 155 K, respectively [53-55]. In the Magnéli series, all except V_7O_{13} (metallic) exhibit a transition from paramagnetic to antiferromagnetic and have an antiferromagnetic ground state at low temperatures. These include V_3O_5, V_4O_7, V_5O_9, V_6O_{11}, V_7O_{13}, V_8O_{15}, and V_9O_{17} with varying phase transition temperatures [56].

The Magnéli series of compounds based on vanadium is a group of highly versatile substances that possess sub-stoichiometric oxygen composition and have a formulation of V_nO_{2n-1} ($3 \leq n \leq 9$). The structure may be traced back to rutile and corundum, where crystallographic shear (CS) planes form as a result of the structural combination of edge-sharing octahedral chains in the rutile structure and face-sharing octahedral links in the corundum structure. These CS planes are characteristic features in early transition metal oxides with low oxygen content, resulting in metal reduction and a rise in charge carrier concentration. The presence of CS planes restricts the mean free path of phonons and reduces thermal conductivity as they interrupt the periodic structure. Moving from V_2O_3 to VO_2, the extremities of the V-O phase diagram of the V_nO_{2n-1} Magnéli series exhibit a reduction in the d-band occupation across the series, thereby altering the electronic properties that can give rise to insulating (V_3O_5), metallic (V_7O_{13}), or semiconducting (V_6O_{11}, V_8O_{15}, V_9O_{17}) behavior at room temperature [57, 58].

Nagasawa et al. [59] discussed the electrical and thermoelectric characteristics of V_nO_{2n-1} (n=3, 4,5,6,7, and 8). The behavior of these compounds at different temperatures is investigated. Notably, V_3O_5 displays semiconductor properties, with its electrical conductivity varying based on temperature, and its anisotropic nature is minimal. V_4O_7 exhibits a transition from metal to semiconductor behavior around 244 K, accompanied by changes in activation energy. Similarly, V_5O_9 and V_6O_{11} undergo metal-semiconductor transitions with varying activation energies and thermoelectric properties. V_7O_{15} maintains metallic conductivity, while V_8O_{15} showcases a metal-semiconductor transition near 70 K. These transitions correlate with magnetic changes in the compounds and potentially indicate first-order transitions. Overall, the study sheds light on the intricate interplay of electronic and magnetic properties in these vanadium oxide compounds. M. Joos et al [57] synthesized V_6O_{11} via SPS and determined the phase purity of 96.64 wt%. The SPS-treated V_6O_{11} material exhibits a maximum PF of $(4.9 \pm 0.8) \times 10^{-5}$ $Wm^{-1}K^{-2}$ and a thermal conductivity κ of (2.72 ± 0.06) $Wm^{-1}K^{-1}$ at a temperature of 600 K.

6. Niobium suboxides Magnéli phases

Niobium suboxides are a class of compounds where the ratio of niobium to oxygen is greater than 2.5 such as $Nb_{25}O_{62}$, $Nb_{47}O_{116}$, $Nb_{22}O_{54}$, and $Nb_{12}O_{29}$ as shown in Fig. 8. They are part of a family of compounds known as crystallographic shear phases of niobium oxide, which have received attention for their unusual electronic and magnetic properties, as well as their performance as intercalation electrode materials for lithium-ion batteries [60]. These compounds feature blocks of niobium-oxygen octahedra as structural units, and this block structure leads to a coexistence of flat and dispersive energy bands, corresponding to localized and delocalized electronic states. Electrons localize in orbitals spanning multiple niobium sites in the plane of the blocks [60].

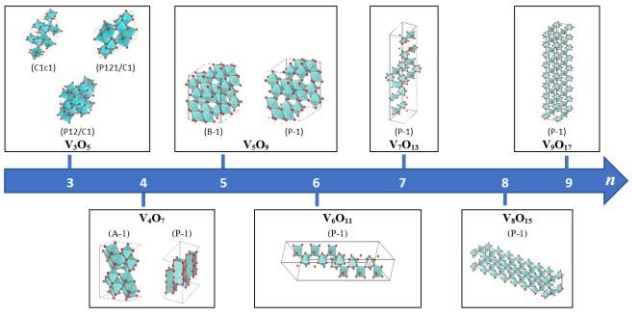

Fig. 7: Crystal structure of Vanadium suboxides

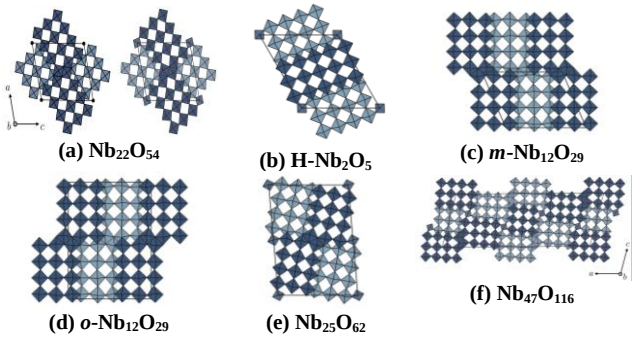

Fig. 8: a) Idealized (left) and locally distorted (right) crystal structure of $Nb_{22}O_{54}$. Crystal structures of b) H-Nb_2O_5, c) monoclinic $Nb_{12}O_{29}$, d) orthorhombic $Nb_{12}O_{29}$, e) $Nb_{25}O_{62}$, and f) $Nb_{47}O_{116}$. Reprinted figure with permission from [60]. https://doi.org/10.1103/PhysRevB.99.075151. Copyright 2023 by the American Physical Society.

Researchers have discovered that achieving such low lattice conductivities in defective oxides can be approached by utilizing crystallographic shear defects and complex block structures. This approach can tune the thermal conductivity in oxides with phonon scattering lengths at the 0.5-5 nanometer length scale, resulting in ZT values as high as 0.21 when measured at 1000K. At 1050K, the thermoelectric figure of merit for the material can be greater than 0.15, and the Seebeck coefficient can be more negative than -80 μV/K. Over a temperature range of 450 to 1050K, the lattice thermal conductivity can be less than 3 $Wm^{-1}K^{-1}$, and the electrical conductivity can be greater than 20000 S/m [61]. Besides the stoichiometric phases Nb_2O_5 and NbO_2, there are many Nb_2O_{5-x} phases [61]. Thermoelectric measurements of NbO_x were shown in Fig. 9. A homologous sequence of structurally similar niobium oxide phases with the general formula $Nb_{3n+1}O_{8n-2}$, n=5, 6, 7, 8 (e.g., $Nb_{16}O_{38}$, $Nb_{19}O_{46}$, $Nb_{22}O_{54}$, $Nb_{25}O_{62}$) can summarize these. In addition, other oxides with the formulas $Nb_{12}O_{29}$ ($12Nb_2O_5$-2O) and $Nb_{94}O_{232}$ ($47Nb_2O_5$-3O) can form [61].

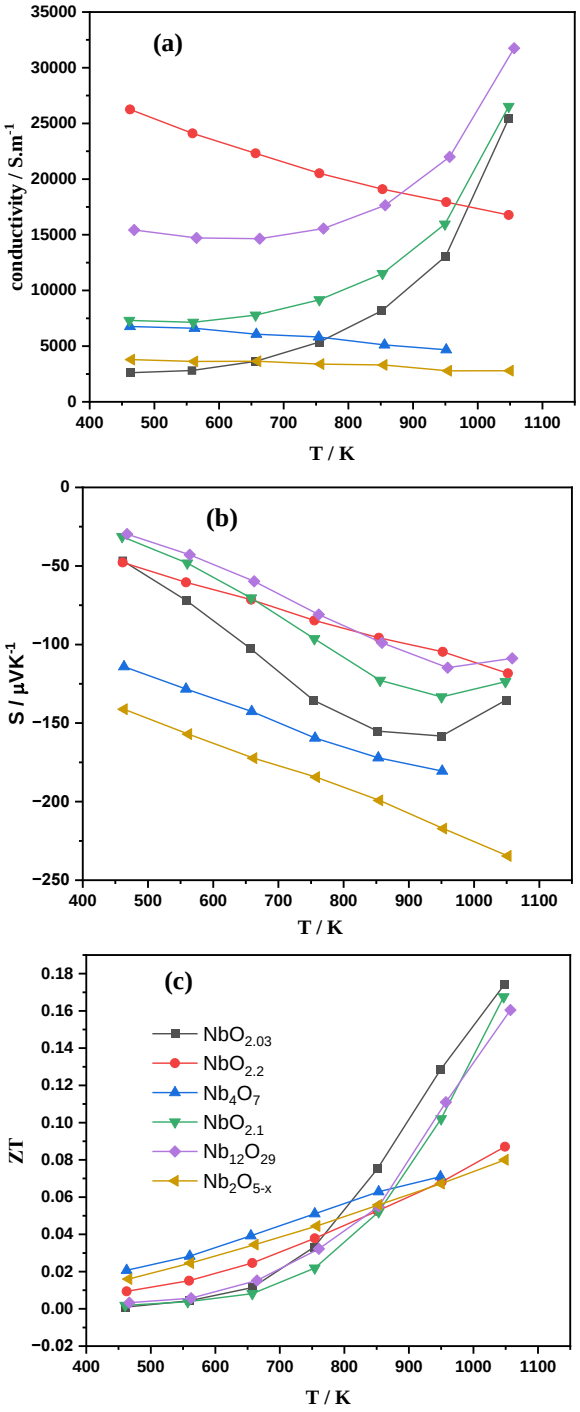

Fig. 9: Temperature dependence (a) electrical conductivity (b) Seebeck coefficient (c) ZT of NbO_x [61].

7. Challenges and Future Developments

Magnéli phases have shown promise as thermoelectric materials, but they also come with limitations and challenges. One challenge is the difficulty in obtaining monophasic materials, as seen with titanium sub-oxides of the Magnéli phase [62]. Also, Most Magnéli series phases, however, are unstable at high temperatures and are oxidized or reduced to nearby metal oxides such as V_nO_{2n-1} phases, eventually providing the compositional end phases VO_2 and V_2O_3 [57]. Synthetic and processing challenges, especially for metastable and nanostructured materials, hinder the advancement of Magnéli phases [57]. Another limitation is the relatively low thermoelectric performance of n-type oxides compared to p-type oxides [63]. However, recent developments have shown that Magnéli oxides can achieve relatively low thermal conductivities and metallic-like electrical conductivities, making them promising n-type thermoelectric [12]. The enhancement of conversion efficiency in thermoelectric materials is challenging, but multiphase thermoelectric materials, including Magnéli phases, provide new approaches to enhance the electronic transport properties [11]. Overall, while Magnéli phases have potential, further research is needed to overcome the challenges and improve their thermoelectric performance.

8. Conclusion:

Magnéli phases are a promising class of thermoelectric materials with a wide range of potential applications. Their high electrical conductivity and low thermal conductivity make them attractive for a variety of high-temperature applications. Magnéli phases of transition metal oxides like TiO_x, WO_x, MoO_x, VO_x, and NbO_x with discussion of their potential application as thermoelectric materials.

However, there are still some challenges that need to be addressed before the Magnéli phases can be fully commercialized. These challenges include optimizing their thermoelectric properties and developing new synthesis methods. Despite these challenges, we believe that Magnéli phases have the potential to revolutionize the field of thermoelectrics. With further research and development, they could become the leading choice for thermoelectric applications in the future.

References:

1. Kieslich, G., et al., *A chemists view: Metal oxides with adaptive structures for thermoelectric applications.* Physica Status Solidi a-Applications and Materials Science, 2016. **213**(3): p. 808-823.
2. Pourkiaei, S.M., et al., *Thermoelectric cooler and thermoelectric generator devices: A review of present and potential applications, modeling and materials.* Energy, 2019. **186**: p. 115849.
3. Slack, G.A. and D. Rowe, *CRC handbook of thermoelectrics*. 1995, CRC press Boca Raton, FL.
4. Jonson, M. and G.D. Mahan, *Mott's formula for the thermopower and the Wiedemann-Franz law.* Physical Review B, 1980. **21**(10): p. 4223-4229.
5. Franz, R. and G. Wiedemann, *Ueber die Wärme-Leitungsfähigkeit der Metalle.* Annalen der Physik, 1853. **165**(8): p. 497-531.
6. Ekren, D., F. Azough, and R. Freer, *2.11 - Oxide thermoelectric materials*, in *Thermoelectric Energy*

Conversion, R. Funahashi, Editor. 2021, Woodhead Publishing. p. 303-331.
7. Brinks, P. and M. Huijben, *14 - Thermoelectric oxides*, in *Epitaxial Growth of Complex Metal Oxides*, G. Koster, M. Huijben, and G. Rijnders, Editors. 2015, Woodhead Publishing. p. 397-441.
8. Ohta, H., K. Sugiura, and K. Koumoto, *Recent progress in oxide thermoelectric materials: p-type Ca3CO4O9 and n-type SrTiO3-*. Inorganic Chemistry, 2008. **47**(19): p. 8429-8436.
9. OHTAKI, M. *Oxide thermoelectric materials: An overview with some historical and strategic perspectives*. in *Oxide thermoelectrics*. 2002.
10. Mele, P., K. Matsumoto, and K. Miyazaki, *Synthesis and characterization of n-type and p-type thermoelectric oxides.* Transactions of the Materials Research Society of Japan, 2010. **35**(1): p. 155-158.
11. Kieslich, G. and W. Tremel, *Magneli oxides as promising n-type thermoelectrics.* Aims Materials Science, 2014. **1**(4): p. 184-190.
12. Malik, H., S. Sarkar, S. Mohanty, and K. Carlson, *Modelling and synthesis of Magnéli Phases in ordered titanium oxide nanotubes with preserved morphology.* Scientific Reports, 2020. **10**(1): p. 8050.
13. Harada, S., K. Tanaka, and H. Inui, *Thermoelectric properties and crystallographic shear structures in titanium oxides of the Magneli phases.* Journal of Applied Physics, 2010. **108**(8).
14. Anderson, J.S. and B.G. Hyde, *On the possible role of dislocations in generating ordered and disordered shear structures.* Journal of Physics and Chemistry of Solids, 1967. **28**(8): p. 1393-1408.
15. Bursill, L.A. and J.S. Anderson, *Crystallographic shear in molybdenum trioxide.* Proceedings of the Royal Society of London. A. Mathematical and Physical Sciences, 1969. **311**(1505): p. 267-290.
16. Stoneham, A.M. and P.J. Durham, *The ordering of crystallographic shear planes: Theory of regular arrays.* Journal of Physics and Chemistry of Solids, 1973. **34**(12): p. 2127-2135.
17. Smith, J.R., F.C. Walsh, and R.L. Clarke, *Electrodes based on Magnéli phase titanium oxides: the properties and applications of Ebonex® materials.* Journal of Applied Electrochemistry, 1998. **28**(10): p. 1021-1033.
18. Walsh, F.C. and R.G.A. Wills, *The continuing development of Magnéli phase titanium sub-oxides and Ebonex® electrodes.* Electrochimica Acta, 2010. **55**(22): p. 6342-6351.
19. Yuan, Z., et al., *Thermoelectric properties of Nb-doped TiO2-δ ceramics reduced at elevated temperature.* Ceramics International, 2017. **43**(17): p. 15454-15458.
20. Andersson, S., B. Collén, U. Kuylenstierna, and A. Magnéli, *Phase analysis studies on the titanium-oxygen system.* Acta chem. scand, 1957. **11**(10): p. 1641-1652.
21. Arif, A.F., et al., *Highly conductive nano-sized Magnéli phases titanium oxide (TiOx).* Scientific Reports, 2017. **7**(1): p. 3646.
22. Kumar, A., N.H. Barbhuiya, and S.P. Singh, *Magnéli phase titanium sub-oxides synthesis, fabrication and its application for environmental remediation: Current status and prospect.* Chemosphere, 2022. **307**: p. 135878.
23. Jayashree, S. and M. Ashokkumar, *Switchable Intrinsic Defect Chemistry of Titania for Catalytic Applications.* Catalysts, 2018. **8**(12): p. 601.
24. Tanaka, K., et al., *Structural Phase Transition between γ-Ti3O5 and δ-Ti3O5 by Breaking of a One-Dimensionally Conducting Pathway*. Crystal Growth & Design, 2015. **15**(2): p. 653-657.
25. Rusakov, A. and G. Zhdanov. *Crystal structure and chemical formula of titanium oxide Ti305 (anosovite)*. in *Dokl. Akad. Nauk SSSR*. 1951.
26. Hodeau, J. and M. Marezio, *Structural aspects of the metal-insulator transitions in (Ti0. 9975V0. 0025) 4O7.* Journal of Solid State Chemistry, 1979. **29**(1): p. 47-62.
27. Marezio, M. and P. Dernier, *The crystal structure of Ti4O7, a member of the homologous series TinO2n− 1.* Journal of Solid State Chemistry, 1971. **3**(3): p. 340-348.
28. Andersson, S. and L. Jahnberg, *Crystal structure studies on the homologous series Ti n O 2n-1, V n O 2n-1 and Ti n-2 Cr 2 O 2n-1.* Ark. Kemi, 1963. **21**(39): p. 413-26.
29. Andersson, S., et al., *The crystal structure of Ti5O9.* Acta chem. scand, 1960. **14**(5): p. 1161-72.
30. Le Page, Y. and P. Strobel, *Structural chemistry of the Magnéli phases TinO2n− 1, 4≤ n≤ 9: II. Refinements and structural discussion.* Journal of Solid State Chemistry, 1982. **44**(2): p. 273-281.
31. Grey, I., et al., *New M3O5-anatase intergrowth structures formed during low-temperature oxidation of anosovite.* Journal of Solid State Chemistry, 2000. **150**(1): p. 128-138.
32. Stoyanov, E., F. Langenhorst, and G. Steinle-Neumann, *The effect of valence state and site geometry on Ti L3,2 and O K electron energy-loss spectra of Ti_xO_y phases.* American Mineralogist, 2007. **92**(4): p. 577-586.
33. Lee, H., S.J. Han, R. Chidambaram Seshadri, and S. Sampath, *Thermoelectric properties of in-situ plasma spray synthesized sub-stoichiometry TiO2−x.* Scientific Reports, 2016. **6**(1): p. 36581.
34. Hao, L., et al., *Magnèli phase TinO2n-1 bulks prepared by SPS followed by carbon reduction and their thermoelectric performance.* Journal of Alloys and Compounds, 2017. **722**: p. 846-851.
35. Pandey, S.J., et al., *Modeling the Thermoelectric Properties of Ti5O9 Magnéli Phase Ceramics.* Journal of Electronic Materials, 2016. **45**(11): p. 5526-5532.
36. Yuan, Z., et al., *Investigation of the thermoelectric properties of reduced Nb-doped TiO2-δ ceramics.* Journal of Alloys and Compounds, 2017. **710**: p. 778-783.
37. Zhou, D., et al., *Preparation of titanium-tantalum-oxygen composite thermoelectric ceramics through high-pressure and high-temperature method.* Journal of Alloys and Compounds, 2022. **918**: p. 165573.
38. Zhou, D., et al., *Preparation of novel titanium-niobium-oxygen composite ceramic with excellent thermoelectric properties using the high-pressure and high-temperature*

method. Journal of the European Ceramic Society, 2022. **42**(12): p. 4980-4986.
39. Mikami, M. and K. Ozaki, *Thermoelectric properties of nitrogen-doped TiO2-x compounds.* Journal of Physics: Conference Series, 2012. **379**(1): p. 012006.
40. Migas, D.B., V.L. Shaposhnikov, and V.E. Borisenko, *Tungsten oxides. II. The metallic nature of Magnéli phases.* Journal of Applied Physics, 2010. **108**(9).
41. Kaiser, F., et al., *Spark Plasma Sintering of Tungsten Oxides WOx (2.50 <= x <= 3): Phase Analysis and Thermoelectric Properties.* Crystals, 2017. **7**(9).
42. Lee, Y.J., T. Lee, and A. Soon, *Phase Stability Diagrams of Group 6 Magneli Oxides and Their Implications for Photon-Assisted Applications.* Chemistry of Materials, 2019. **31**(11): p. 4282-4290.
43. Tran, N.Q.M., M. Ohtaki, and K. Suekuni, *Rapid Synthesis of W_18O_49 via Reactive Spark Plasma Sintering with Controlled Anisotropic Thermoelectric Properties.* 2021.
44. Tran, N.Q.M., M. Ohtaki, and K. Suekuni, *High-temperature thermoelectric performance of (W1−xTix)18O49.* Journal of the European Ceramic Society, 2022. **42**(4): p. 1486-1492.
45. Kieslich, G., et al., *Enhanced thermoelectric properties of the n-type Magnéli phase WO2.90: reduced thermal conductivity through microstructure engineering.* Journal of Materials Chemistry A, 2014. **2**(33): p. 13492-13497.
46. Magneli, A., N. Hofman-Bang, and P. Gjertsen, *The Crystal Structures of Mo9O26 (beta'-Molybdenum Oxide) and Mo8O23 (beta-molybdenum Oxide).* Acta Chemica Scandinavica, 1948. **2**: p. 501-517.
47. Kihlborg, L., et al., *Stabilization of the Tunnel Structure of Mo5O14 by Partial Metal Atom Substitution.* Acta Chemica Scandinavica, 1969. **23**: p. 1834-1835.
48. Kihlborg, L., *The crystal structure of Mo17O47.* Acta Chem. Scand, 1960. **14**(7).
49. Yang, F., et al., *Enhanced electrocatalytic performance for methanol oxidation with a Magnéli phase molybdenum oxide/Pt-black composite.* Journal of Molecular Catalysis A: Chemical, 2015. **400**: p. 7-13.
50. Kihlborg, L., *Least squares refinement of crystal structure of molybdenum trioxide.* Arkiv for Kemi, 1963. **21**(4): p. 357-+.
51. Khilla, M.A., Z.M. Hanafi, B.S. Farag, and A. Abu-el Saud, *Transport properties of molybdenum trioxide and its suboxides.* Thermochimica Acta, 1982. **54**(1): p. 35-45.
52. Kaiser, F., M. Schmidt, Y. Grin, and I. Veremchuk, *Molybdenum Oxides MoOx: Spark-Plasma Synthesis and Thermoelectric Properties at Elevated Temperature.* Chemistry of Materials, 2020. **32**(5): p. 2025-2035.
53. Hu, P., et al., *Vanadium Oxide: Phase Diagrams, Structures, Synthesis, and Applications.* Chemical Reviews, 2023. **123**(8): p. 4353-4415.
54. Kosuge, K., T. Takada, and S. Kachi, *Phase Diagram and Magnetism of V2O3–V2O5 System.* Journal of the Physical Society of Japan, 1963. **18**(2): p. 318-319.
55. Heidemann, A., K. Kosuge, Y. Ueda, and S. Kachi, *Hyperfine interaction in V3O7.* Phys Status Solidi A, 1977. **39**(1): p. K37-K40.
56. Schwingenschlögl, U. and V. Eyert, *The vanadium Magnéli phases VnO2n-1.* Annalen der Physik, 2004. **516**(9): p. 475-510.
57. Joos, M., et al., *Spark Plasma Sintering (SPS)-Assisted Synthesis and Thermoelectric Characterization of Magnéli Phase V6O11.* Inorganic Chemistry, 2018. **57**(3): p. 1259-1268.
58. Idlis, B.G. and Y.V. Kopaev, *On the theory of phase transitions in vanadium oxides VnO2n-1 (magneli phases).* Solid State Communications, 1983. **45**(3): p. 301-304.
59. Nagasawa, K., Y. Bando, and T. Takada, *Growth and Electrical Properties of V [n] O_2 [n]$_{-1}$ (n= 3, 4,..., 8) Single Crystals.* Bulletin of the Institute for Chemical Research, Kyoto University, 1972. **49**(5): p. 322-341.
60. Koçer, C.P., K.J. Griffith, C.P. Grey, and A.J. Morris, *First-principles study of localized and delocalized electronic states in crystallographic shear phases of niobium oxide.* Physical Review B, 2019. **99**(7): p. 075151.
61. Backhaus-Ricoult, M., *Niobium oxide-based thermoelectric composites*. 2013, Google Patents.
62. Fortulan, R. and S.A. Yamini, *Recent Progress in Multiphase Thermoelectric Materials.* Materials, 2021. **14**(20).
63. Fan, Y.C., et al., *Preparation of monophasic titanium sub-oxides of Magneli phase with enhanced thermoelectric performance.* Journal of the European Ceramic Society, 2018. **38**(2): p. 507-513.